HHS Public Access

Author manuscript

Int J Radiat Oncol Biol Phys. Author manuscript; available in PMC 2019 November 15.

Published in final edited form as:

Int J Radiat Oncol Biol Phys. 2018 November 15; 102(4): 841–847. doi:10.1016/j.ijrobp.2018.04.067.

Velocity-Based Adaptive Registration and Fusion for Fractionated Stereotactic Radiosurgery Using the Small Animal Radiation Research Platform

Paul J. Black[#1], **Deborah R. Smith**[#1], **Kunal Chaudhary**[1], **Eric P. Xanthopoulos**[1], **Christine Chin**[1], **Catherine S. Spina**[1], **Mark E. Hwang**[1], **Mark Mayeda**[1], **Yi-Fang Wang**[1], **Eileen P. Connolly**[1], **Tony J. C. Wang**[1,3,4], **Cheng-Shie Wuu**[1], **Tom K. Hei**[1,2], **Simon K. Cheng**[#1,*], and **Cheng-Chia Wu**[#1,*]

[1.)]Department of Radiation Oncology, Columbia University Medical Center, New York, NY 10032

[2.)]Center for Radiological Research, Columbia University, New York, NY 10032

[3.)]Department of Neurological Surgery, Columbia University Medical Center, New York, NY 10032

[4.)]Herbert Irving Comprehensive Cancer Center, Columbia University Medical Center, New York, NY 10032

[#] These authors contributed equally to this work.

Summary:

Fractionated MRI-guided treatment planning using the Small Animal Radiation Research Platform (SARRP) can be complex due to MRI registration with cone-beam CT images. Using Velocity, we have developed a novel preclinical method for murine image fusion and adaptable registration to facilitate fractionated radiation treatment planning. To the best of our knowledge, this is the first study to apply clinical treatment planning software toward SARRP-based treatment planning to conduct translational research using animals.

Abstract

Purpose: To implement Velocity-based image fusion and adaptive deformable registration to enable treatment planning for preclinical murine models of fractionated stereotactic radiosurgery (fSRS) using the Small Animal Radiation Research Platform (SARRP).

Methods and Materials: C57BL6 mice underwent three unique cone-beam computed tomography (CBCT) scans: two in the prone position and a third supine. A single T1-weighted post-contrast Magnetic Resonance Imaging (MRI) series of a murine metastatic brain tumor model was selected for MRI-to-CBCT registration and gross tumor volume (GTV) identification. Two

[*]Co-corresponding authors: Cheng-Chia Wu, Department of Radiation Oncology, Columbia University Medical Center, 622 West 168th Street, BNH B-11, New York, NY 10032, Telephone: 212-305-7077, chw9088@nyp.org, Simon K. Cheng, Department of Radiation Oncology, Columbia University Medical Center, 622 West 168th Street, BNH B-11, New York, NY 10032, Telephone: 212-305-3356, sc3225@cumc.columbia.edu.

arms were compared: Arm 1, where we performed three individual MRI-to-CBCT fusions using rigid registration, contouring GTVs on each, and Arm 2, where we performed MRI-to-CBCT fusion and contoured GTV on the first CBCT followed by Velocity-based adaptive registration. The first CBCT and associated GTV were exported from MuriPlan (Xstrahl) into Velocity (Varian). In Arm 1, the second and third CBCTs were exported similarly along with associated GTVs (Arm 1), while in Arm 2, the first (prone) CBCT was fused separately to the second (prone) and third (supine) CBCTs, performing deformable registrations on initial CBCTs and applying resulting matrices to the contoured GTV. Resulting GTVs were compared between Arms 1 and 2.

Results: Comparing GTV overlays using repeated MRI fusion and GTV delineation (Arm 1) versus those of Velocity-based CBCT and GTV adaptive fusion (Arm 2), mean deviations ± standard deviation in the axial, sagittal, and coronal planes were 0.46±0.16, 0.46±0.22, and 0.37±0.22 mm for prone-to-prone and 0.52±0.27, 0.52±0.36, and 0.68±0.31 mm for prone-to-supine adaptive fusions, respectively.

Conclusion: Velocity-based adaptive fusion of CBCTs and contoured volumes allows for efficient fSRS planning using a single MRI-to-CBCT fusion. This technique is immediately implementable on current SARRP systems, facilitating advanced preclinical treatment paradigms using existing clinical treatment planning software.

Introduction:

Radiation therapy plays an essential role in the management of brain metastases. With modern clinical advances in radiotherapy, stereotactic radiosurgery (SRS) has emerged as standard-of-care treatment for select patients with limited brain metastases.[5,8] SRS treatments are traditionally delivered using a single fraction. However, both modern linear accelerator-based treatments and the Gamma Knife Icon allow for fractionated SRS (fSRS) in appropriate patients (e.g., for larger tumors or postoperative cavities) who may benefit. [12,13,16]

Given growing interest in expanding indications for SRS-based treatments, including potential combinations with immunotherapy, preclinical models are needed to evaluate novel roles for singlefractionated and fractionated SRS. The SARRP (Xstrahl, Suwanee, GA) is a small-animal irradiator capable of advanced radiation treatment planning and delivery. Preclinical small animal models of MRI-guided radiotherapy using the SARRP have been successfully established for intracranial, flank and abdominal tumors using various strategies including usage of immobilization devices, fiducial marker placement and MRI-only based treatment planning.[2,3,6,10,11] While SARRP-based, MRI-guided, single-fraction SRS for brain tumors achieves precise dose delivery [18], GTV identification and treatment planning for fractionated SARRP treatments currently requires repeat MRI fusion and registration to account for shifts in daily positioning, which is challenging and limits clinical applicability. Moreover, questions remain whether advanced clinical treatment planning technologies can be successfully integrated into existing workflows for small animal treatment planning to further advance sophistication and clinical relevance of SARRP-based treatment delivery for preclinical models of radiation therapy.

Therefore, the purpose of this study was to implement adaptable registration using deformable image registration with Velocity (Varian Medical Systems, Inc., Palo Alto, CA) into existing workflows for SARRP-based small animal treatment delivery to establish a preclinical murine model for SARRP-based fSRS. Here, we demonstrate that Velocity-based CBCT-to-CBCT image fusion and deformable registration can successfully account for day-to-day treatment setup variability and transform target volumes to allow for SARRP-based murine fSRS.

Material/Methods:

Experiments were conducted according to our Institutional Animal Care and Use Committee (IACUC). Seven-week old male C57BL6 mice (Jackson Laboratory, Bar Harbor, ME) were anesthetized with xylazine and ketamine. A representative post-contrast T1-weighted MRI scan of a mouse with a single brain metastasis from previous work was selected for MRI-to-CBCT rigid registration (Detailed information regarding generation of the orthotopic murine model provided in XXXXX et al., IJROBP 2017) [18]. Four mice each underwent three CBCT scans, two in the prone position (Scans A and B) and one supine (Scan C). To simulate fractionated treatment, mice were successively removed from the treatment stage and repositioned before each CBCT scan. We investigated both prone-prone (A-B) and prone-supine (A-C) variations to assess limitations of Velocity-based adaptive registration. Manual MRI-to-CBCT rigid registration was performed in Muriplan (Xstrahl). A five-point positioning system using bilateral orbits, auditory canals and the cribiform plate as anatomical landmarks, along with consideration of bony anatomy of the cranium, was used to verify correct co-registration. CBCTs and associated GTVs were exported from Muriplan into Velocity. Experiments were performed in duplicate by two independent users. Details regarding image and structure set handling and transformations using custom-written MATLAB scripts are provided in the Supplement. We compared correspondence of GTVs between two experimental arms (Figure 1): Arm 1, where three individual MRI-to-CBCT fusions were performed using rigid registration with GTVs contoured on each CBCT, and Arm 2, where MRI-to-CBCT fusion and GTV contouring were performed for only Scan A, using Velocity-based deformable registration with GTV adaptation for successive CBCT scans (Scans B and C). Briefly, in Arm 2 (Velocity-based adaptive registration), the first (prone) CBCT (Scan A) was separately fused to the second (Scan B) and third (Scan C) CBCTs. Deformable registrations were performed on initial CBCTs (Scan A), and resulting transformation matrices were applied to the corresponding GTVs. Specifically, Scan B or C was registered as the primary image and Scan A (along with GTV) as the secondary image. Rigid registration was first performed with Scan A to bring primary and secondary images into close proximity, followed by deformable registration. The transformation matrix was then applied to the GTV from Scan A. We compared independently-contoured GTVs from Scans B and C in Arm 1 (manual MRI-CBCT rigid registration in Muriplan and GTV contouring on each scan) to Velocity-adapted GTVs applied to successive CBCTs (Scans B and C) from Scan A in Arm 2 by comparing GTV centroid shifts between methods in the axial, sagittal and coronal planes. The related-samples Wilcoxon signed rank test was used to compare mean vector shifts of GTV centroids between prone and supine scans between Arm 1 and Arm 2 (e.g., for target volumes repeatedly contoured using manual CBCT-to-

MRI rigid registration versus Velocity-based adaptive fusion of GTVs). P values less than 0.05 were considered statistically significant. Both intra-user and inter-user GTV variability were characterized using descriptive statistics.

Results:

Velocity effectively performed all murine CBCT and GTV registrations (Figures 2 and 3). Figure 2 displays CBCT and GTV positions in Arm 2 before deformable registration from Scan A (red) and Scan B (green). As shown in Figure 3, Velocity-based application of the associated transformation matrix to the GTV from Scan A resulted in strong co-localization with the corresponding GTV from Scan B. Even for successive CBCT scans with radical position shifts (e.g., prone-to-supine between Scans A and C), Velocity performed deformable registration with high coincidence.

Deviations of the GTV centroids between Arm 1 (manual MRI-to-CBCT and repeated GTV contouring) and Arm 2 (Velocity-based deformable registration) in all three planes (axial, sagittal and coronal) were compared for all transformed GTVs (Table 1). Scan A-to-B (prone-to-prone) average deviations between arms were 0.46±0.16, 0.46±0.22, and 0.37±0.22 mm in the axial, sagittal and coronal planes, respectively. Scan A-to-C (prone-to-supine) deviations were 0.52±0.27, 0.52±0.36, and 0.68±0.31 mm, respectively. However, comparison of Arms 1 and 2 (manual CBCT-MRI rigid registration versus Velocity-based adaptive fusion) by comparing mean GTV centroid vector shifts between prone and supine scans across both methods revealed no statistically significant difference between Arm 1 and Arm 2 ($p = 0.327$). GTV centroid variability (both inter-operator and intra-operator) are available in Supplementary Tables 1 and 2, respectively. Dosimetric analysis examining overlaps in target coverage between the two methods was also performed by designing an AP-PA plan to the Velocity-deformed GTV to evaluate relative coverage of the Muriplan MR-fusion derived GTV (Supplementary Figure 1). Overall, dosimetric analysis demonstrated high correspondence of GTV coverage between methods (Supplementary Table 3. As demonstrated in Figure 4, final adaptive registration-transformed GTVs (red) were successfully exported from Velocity and imported into MuriPlan for treatment planning, which corresponded well with repeated MRI-guided delineation of GTVs (green).

Discussion:

This study demonstrates feasibility of Velocity-based adaptation of SARRP treatment planning to allow for preclinical murine models of fractionated SRS. Through deformable registration and associated transformation matrices, this technique successfully accounts for inter-fraction GTV position changes. Our results suggest that 0.5 mm planning target volume expansions sufficiently account for associated uncertainty. Given that multiple MRI acquisitions are both expensive and time-consuming, Velocity-based deformable registration of CBCT images provide an appropriate alternative with excellent dosimetric coverage for precise delivery of fractionated MRI-guided treatment delivery in small animal models. After initial manual CBCT-to-MRI coregistration and GTV contouring, the current workflow for adaptive registration for successive CBCT scans can be completed in approximately 20 minutes. However, limitations include lack of full automatization of steps

within our workflow (e.g., CT intensity values of CBCTs from Muriplan must be converted before Velocity importation, and transferring images between software platforms still requires manual image import/export of images). Future work will include automation of additional steps in our current workflow to streamline this process (including creation of a direct link between the Velocity database and 3DSlicer to efficiently push images). As compared with prior studies of MRI-guided fractionated radiation delivery, this technique is easily implementable using existing treatment planning software and can also be used synergistically with immobilization devices and fiducials.

Radiation therapy holds exceptional promise toward enhancing the efficacy of immuno-oncology-based treatments [1]. Both preclinical and clinical findings suggest that radiation can induce abscopal effects through immune sensitization, and immune checkpoint inhibition with concurrent SRS may improve outcomes in the setting of brain metastases. [9,14] [7,17]. Preclinical models for both accurate and clinically applicable delivery of radiation therapy are essential for determining the optimal dose and fractionation schemes to elicit such effects.[15]

This technique establishes a clinically-relevant preclinical model for murine MRI-guided fractionated SRS and also offers many other exciting possibilities for advancing preclinical radiation research, including PET/CT adaptive fusion for targeted therapy using spontaneous metastatic mouse models.[4] Here, we demonstrate that Velocity-based adaptive registration can be easily incorporated into the conventional Muriplan workflow. To our knowledge, this represents the first study to demonstrate feasibility of applying clinical image registration software toward SARRP-based murine treatment planning.

Supplementary Material

Refer to Web version on PubMed Central for supplementary material.

Acknowledgement:

This study was supported by the ASTRO 2016 Residents/Fellows in Radiation Oncology Research Seed Grant, the Irving Institute Imaging Pilot Award, Louis V. Gerstner, Jr. Scholar Award, and the NIH Biomedical Research Support Shared Instrumentation Grant 1S10OD010631-01A1.

References

[1]. Antonia SJ, et al. Durvalumab after chemoradiotherapy in stage iii non-small-cell lung cancer. The New England journal of medicine 2017;377:1919–1929. [PubMed: 28885881]

[2]. Baumann BC, et al. An integrated method for reproducible and accurate image-guided stereotactic cranial irradiation of brain tumors using the small animal radiation research platform. Translational oncology 2012;5:230–237. [PubMed: 22937174]

[3]. Bolcaen J, et al. Mri-guided 3d conformal arc micro-irradiation of a f98 glioblastoma rat model using the small animal radiation research platform (sarrp). Journal of neuro-oncology 2014;120:257–266. [PubMed: 25069566]

[4]. Cho JH, et al. Akt1 activation promotes development of melanoma metastases. Cell reports 2015;13:898–905. [PubMed: 26565903]

[5]. Citrin DE. Recent developments in radiotherapy. The New England journal of medicine 2017;377:2200–2201.

[6]. Corroyer-Dulmont A, et al. Mri-guided radiotherapy of the sk-n-sh neuroblastoma xenograft model using a small animal radiation research platform. Br J Radiol 2017;90:20160427. [PubMed: 27524406]

[7]. Demaria S, Coleman CN, Formenti SC. Radiotherapy: Changing the game in immunotherapy. Trends in cancer 2016;2:286–294. [PubMed: 27774519]

[8]. Garrett MD, et al. Radiation therapy for the management of brain metastases. American journal of clinical oncology 2016;39:416–422. [PubMed: 27213494]

[9]. Goldberg SB, et al. Pembrolizumab for patients with melanoma or non-small-cell lung cancer and untreated brain metastases: Early analysis of a non-randomised, open-label, phase 2 trial. The Lancet. Oncology 2016;17:976–983. [PubMed: 27267608]

[10]. Gutierrez S, Descamps B Vanhove C. Mri-only based radiotherapy treatment planning for the rat brain on a small animal radiation research platform (sarrp). PloS one 2015;10:e0143821. [PubMed: 26633302]

[11]. Kersemans V, et al. An efficient and robust mri-guided radiotherapy planning approach for targeting abdominal organs and tumours in the mouse. PloS one 2017;12:e0176693. [PubMed: 28453537]

[12]. Kim JW, et al. Fractionated stereotactic gamma knife radiosurgery for large brain metastases: A retrospective, single center study. PloS one 2016;11:e0163304. [PubMed: 27661613]

[13]. Stieler F, et al. Adaptive fractionated stereotactic gamma knife radiotherapy of meningioma using integrated stereotactic cone-beam-ct and adaptive re-planning (a-gkfsrt). Strahlentherapie und Onkologie : Organ der Deutschen Rontgengesellschaft … [*et al*] 2016;192:815–819.

[14]. Tallet AV, et al. Combined irradiation and targeted therapy or immune checkpoint blockade in brain metastases: Toxicities and efficacy. Annals of oncology : official journal of the European Society for Medical Oncology 2017;28:2962–2976. [PubMed: 29045524]

[15]. Vanpouille-Box C, et al. DNA exonuclease trex1 regulates radiotherapy-induced tumour immunogenicity. Nature communications 2017;8:15618.

[16]. Wegner RE, et al. Fractionated stereotactic radiosurgery for large brain metastases. American journal of clinical oncology 2015;38:135–139. [PubMed: 23563213]

[17]. Weichselbaum RR, et al. Radiotherapy and immunotherapy: A beneficial liaison? Nature reviews. Clinical oncology 2017;14:365–379.

[18]. Cho JH, Robinson JP, Arave RA, et al. AKT1 activation promotes development of melanoma metastases. Cell Rep 2015;13:898–905. [PubMed: 26565903]

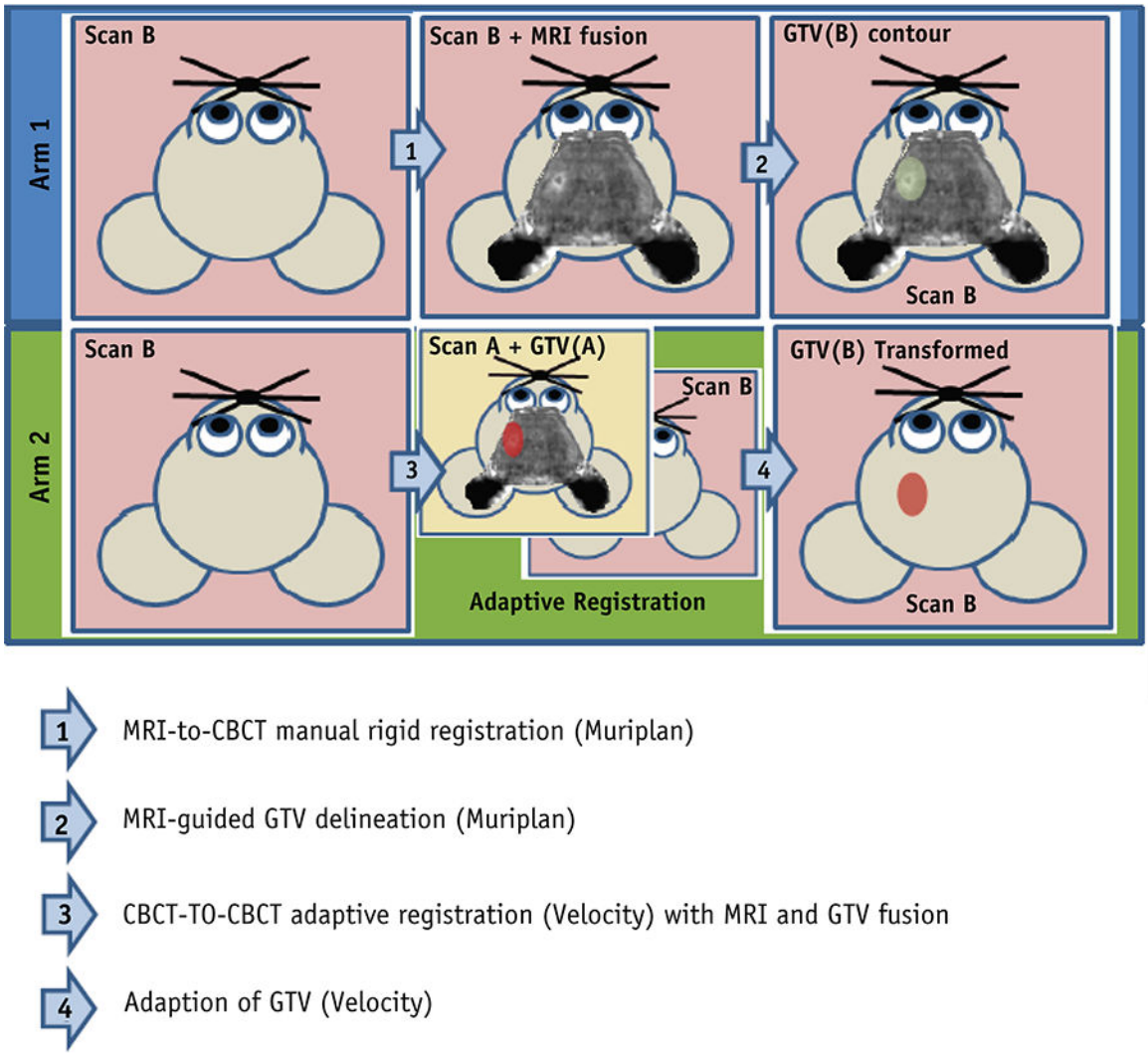

Figure 1:
Overview of Experimental Design. In Arm 1 (blue box), individual MRI-to-CBCT rigid registrations were performed and GTVs were contoured for each successive scan (depicted in green). In Arm 2 (Green Box), MRI-to-CBCT fusion and GTV contouring were performed using Scan A. Velocity-based adaptive registration of CBCTs from Scan A to B and Scan A to C were performed to generate Velocity-adapted GTVs for Scans B and C (red).

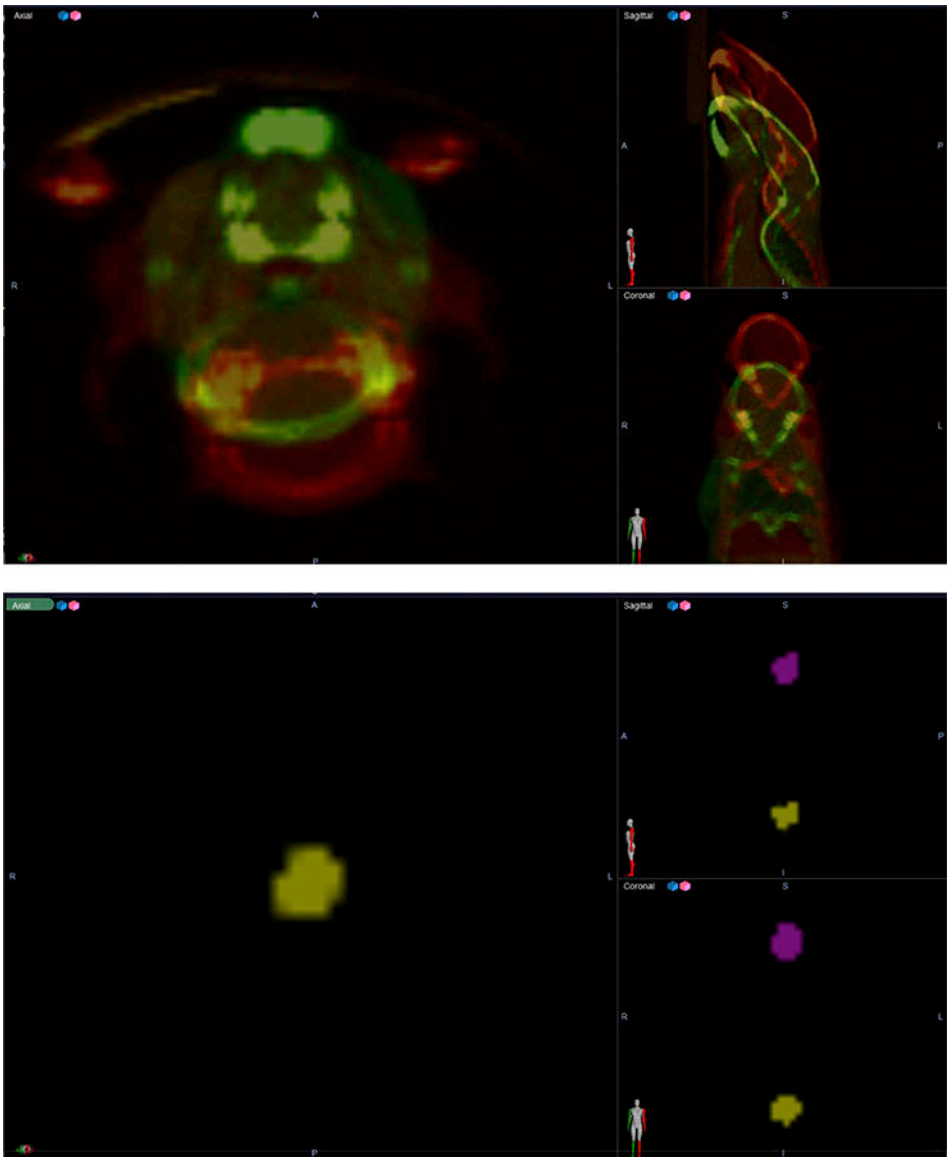

Figure 2:
Two independent CBCTs and GTVs before adaptive registration in Velocity.

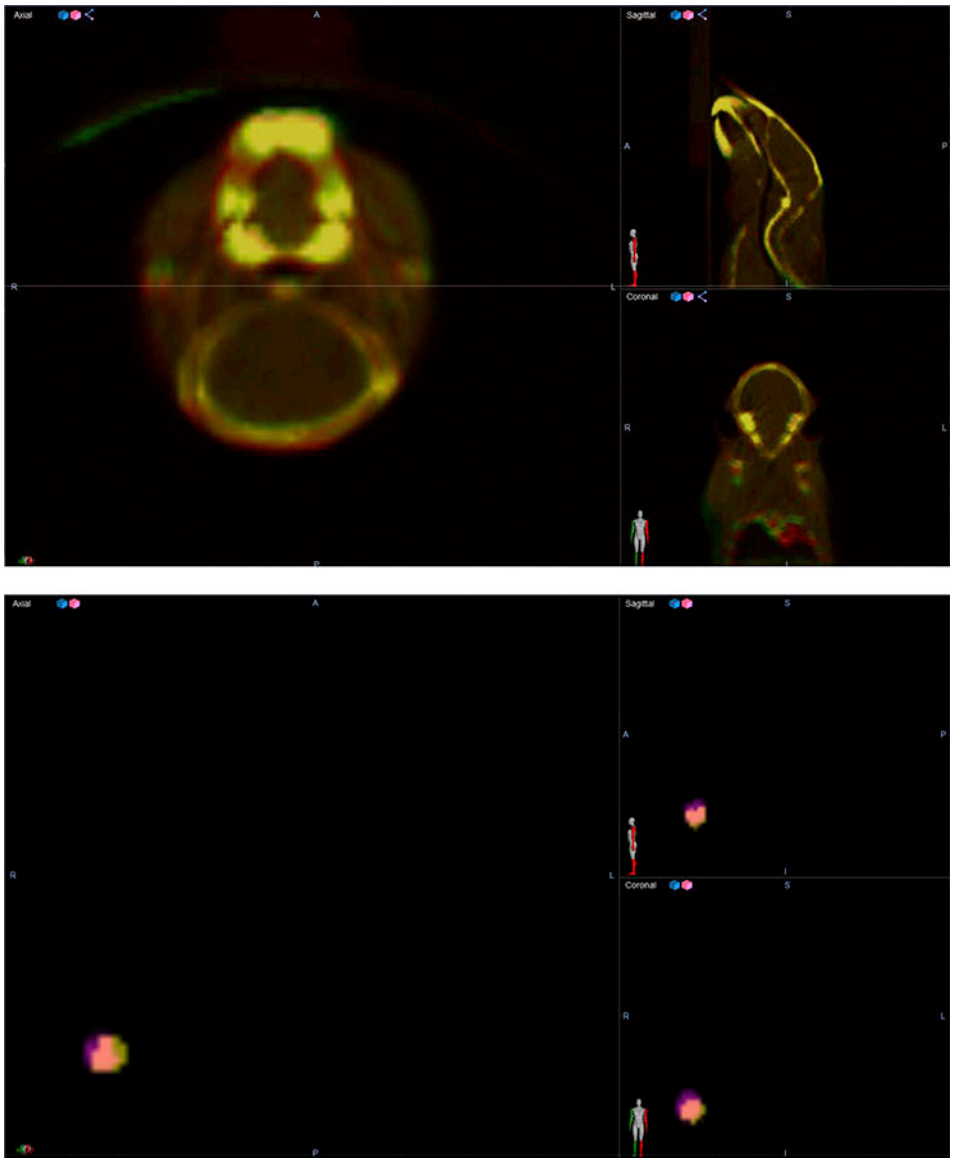

Figure 3:
Two independent CBCTs and GTVs after adaptive registration in Velocity.

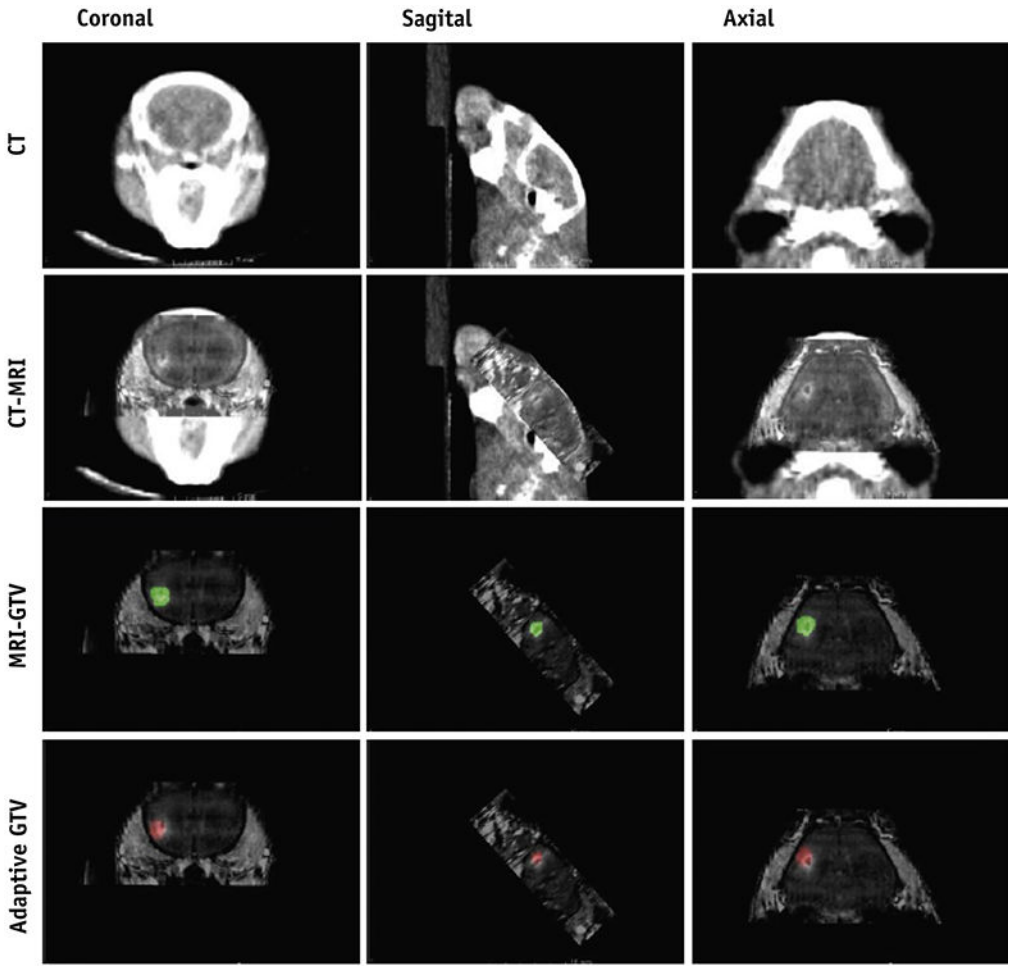

Figure 4:
MuriPlan display of MRI-guided delineation of GTV (green) versus adaptive registration transformed GTV (red)

Table 1:

Deviation of GTV Centroid Between ARM 1 and 2

Comparison	Axial	Sagittal	Coronal	Total Vector
Prone to Prone (A to B)	0.46±0.16	0.46±0.22	0.37±0.22	0.78±0.09
Prone to Supine (A to C)	0.52±0.27	0.52±0.36	0.68±0.31	1.05±0.15